ADVANCED FUNCTIONAL MATERIALS
www.afm-journal.de

Submillimeter-Scale Superlubric Triboelectric Nanogenerator

Tianzhao Bu, Wenli Deng, Yaoyao Liu, Zhong Lin Wang, Xinchun Chen,* and Chi Zhang**

Triboelectric nanogenerator (TENG) for mechanical energy harvesting has been regarded as one of the most prospective energy technologies for the new era. However, inevitable material wear during triboelectrification results in output reduction and even failure of the TENG. In this work, a submillimeter-scale superlubric TENG (SS-TENG) is reported that enables ultra-low friction coefficient (μ) and stable power generation. By using the micro/nano-processing technology, the interdigital electrodes are embedded into the dielectric layer as a flat surface, on which the highly-hydrogenated diamond-like carbon (PLC) is deposited as the triboelectric layer to effectively reduce the friction coefficient. The frictional properties are systematically investigated at different parameters, in which a submillimeter-scale (130 µm) superlubricity state ($\mu = 0.0084$) is achieved at 4 N, 2 Hz and nitrogen atmosphere. Meanwhile, the SS-TENG has a maximum power density of 3 mW m^{-2}, which can remain stable at the superlubric condition. This work has first realized the freestanding-mode superlubric TENG in submillimeter scale and provided a viable strategy for the development of long-lifetime TENG, which may have great applications in frictional energy recovery from mechanical components, human joint motion, and the natural environment.

1. Introduction

Mechanical energy as a clean energy source is widely distributed in the human body and the natural environment.[1–5] Harvesting mechanical energy from human kinetic energy and environmental mechanical energy is promising for solving the energy problem in the era of Internet of things (IoTs).[6–10] Since 2012, triboelectric nanogenerator (TENG) an emerging energy technology has been invented to convert mechanical energy into electricity.[11–15] Due to the diverse working modes, the TENG has been demonstrated to effectively harvest various mechanical energy including human motion energy, vibration energy, wind energy, raindrop energy, and water wave energy.[16–20] However, friction-induced wear is inevitable when the TENG works, which seriously affects the output performance and even leads to the failure of TENG.[21] Thus, wear reduction is the key technology for the long lifetime of TENG.

In recent years, several strategies have been proposed to improve the wear resistance of TENG.[22–24] By structure design, TENG is allowed to work in non-contact mode for a long time. At this time, the output of TENG is generated by electrostatic induction, which gradually decays due to charge dissipation.[25] Hence, contact friction is necessary for triboelectrification to replenish the charges of TENG. Wear-resistant materials can be used as triboelectric layers or by adding lubricants between friction interfaces to reduce wear.[26] However, these methods cannot reduce the coefficient of friction sufficiently, leading to wear has a relatively large impact on the lifetime of TENG. Long-lifetime TENG requires both contact friction for triboelectrification and ultra-low coefficient of friction to reduce wear. Thus, achieving the superlubric triboelectric

T. Bu, Y. Liu, Z. L. Wang, C. Zhang
CAS Center for Excellence in Nanoscience
Beijing Key Laboratory of Micro-Nano Energy and Sensor
Beijing Institute of Nanoenergy and Nanosystems
Chinese Academy of Sciences
Beijing 101400, P. R. China
E-mail: zlwang@gatech.edu; czhang@binn.cas.cn
T. Bu, Y. Liu, Z. L. Wang, C. Zhang
School of Nanoscience and Engineering
University of Chinese Academy of Sciences
Beijing 100049, P. R. China

The ORCID identification number(s) for the author(s) of this article can be found under https://doi.org/10.1002/adfm.202404007

DOI: 10.1002/adfm.202404007

T. Bu
Flexible Electronics Research Center
State Key Laboratory of Intelligent Manufacturing Equipment and Technology, School of Mechanical Science and Engineering
Huazhong University of Science and Technology
Wuhan, Hubei 430074, China
W. Deng, X. Chen
State Key Laboratory of Tribology in Advanced Equipment
Tsinghua University
Beijing 100084, P. R. China
E-mail: chenxc1213@mail.tsinghua.edu.cn
Z. L. Wang, C. Zhang
Guangzhou Institute of Blue Energy
Knowledge City
Huangpu, Guangzhou 510555, P. R. China

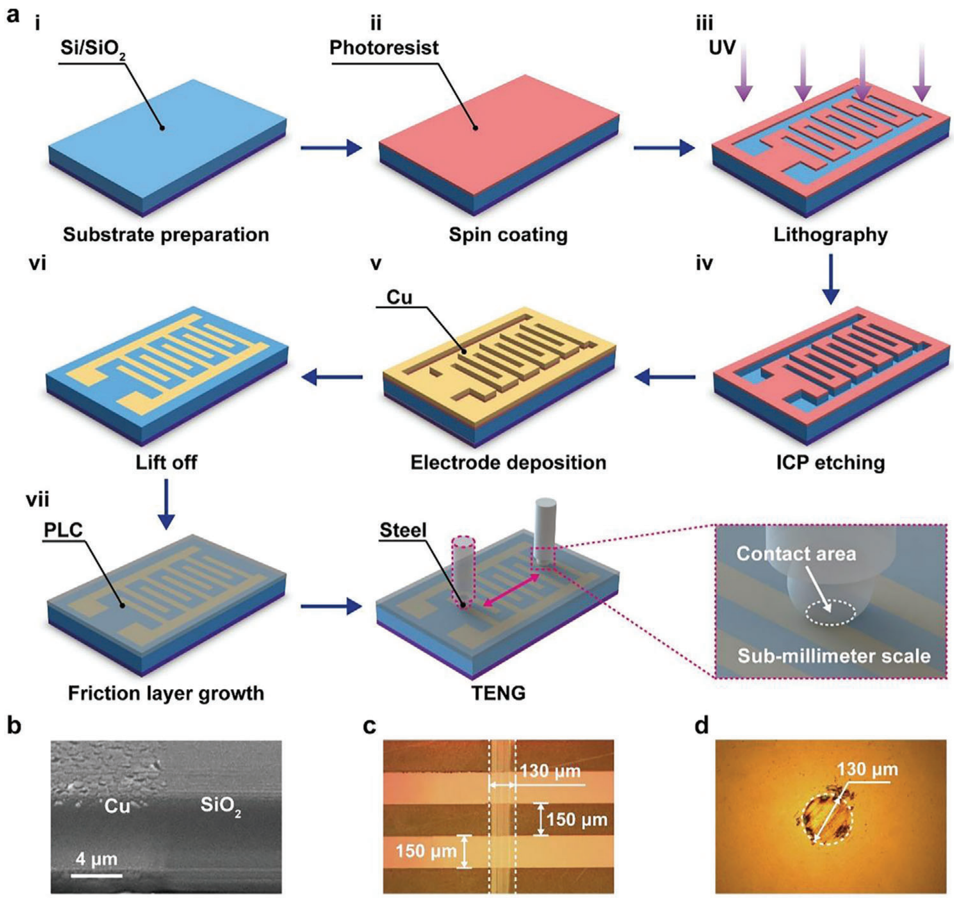

Figure 1. Overview of the SS-TENG. a) Fabrication and structure of the SS-TENG. b) SEM image of the cross-sectional SS-TENG. Optical microscope images of the wear trace on the c) PLC film and the d) steel ball.

interface is the ideal solution for long-lifetime TENG. Huang and co-authors have reported an AFM-based superlubric generator, which is in a microscale.[27] A macroscale superlubric generator was developed by the tribovoltaic effect, in which semiconductor materials are indispensable.[28] This dependency limits the application of superlubric tribovoltaic generators due to the difficulty and high cost of semiconductor processing and manufacturing. Thus, triboelectrification to generate surface charge, superlubric interface to reduce wear, and electrostatic induction to output electricity are the ideal solutions for long-lifetime TENG.

Diamond-like carbon (DLC) films are reported to have a complex structure. Diamond has sp3 carbons with a crystalline structure. By contrast, graphite has layers of sp2 hybridized carbons. The structure of DLC is reported to be an amorphous mixture of both sp2 and sp3 carbon, with the proportion of sp2 and sp3 carbons important in determining the properties of the DLC, such as its mechanical hardness and chemical inertness. On this basis, the DLC films are always used to reduce friction and help prevent wear.[29] Here, a submillimeter-scale superlubric TENG (SS-TENG) is developed that enables ultra-low friction coefficient and stable power generation. By using the micro/nano-processing technology, the interdigital electrodes were embedded into the dielectric layer as a flat surface, on which the highly-hydrogenated diamond-like carbon (PLC) was deposited as the triboelectric layer to effectively reduce the friction coefficient. The frictional properties were systematically investigated at different parameters, in which a submillimeter-scale (130 μm) superlubric condition ($\mu = 0.0084$) was achieved at 4 N, 2 Hz, and N_2 atmosphere. Meanwhile, SS-TENG has a maximum power density of 3 mW m^{-2}, which can remain stable under the superlubric condition. This work has first realized the freestanding-mode superlubric TENG in the submillimeter scale and provided a viable strategy for the development of long-lifetime TENG. Based on the ultralow coefficient of friction (COF), the SS-TENG may have potential applications in industrial mechanical components, in which friction is inevitable and causes significant energy loss. For example, the SS-TENG can serve as embedded devices in bearings for long-time friction energy harvesting to reduce energy loss.

2. Results

The SS-TENG is fabricated by traditional micro/nano-processing technology (**Figure 1**a), in which a SiO_2 layer is first etched with the shape of interdigital electrodes (Figure 1a i–iv) and Cu is then filled in the recess to form a flat surface (Figure 1a v,vi). DLC film is the key component of SS-TENG. In this work, four different kinds of DLC including PLC (Hydrogen-rich polymer-like DLC),

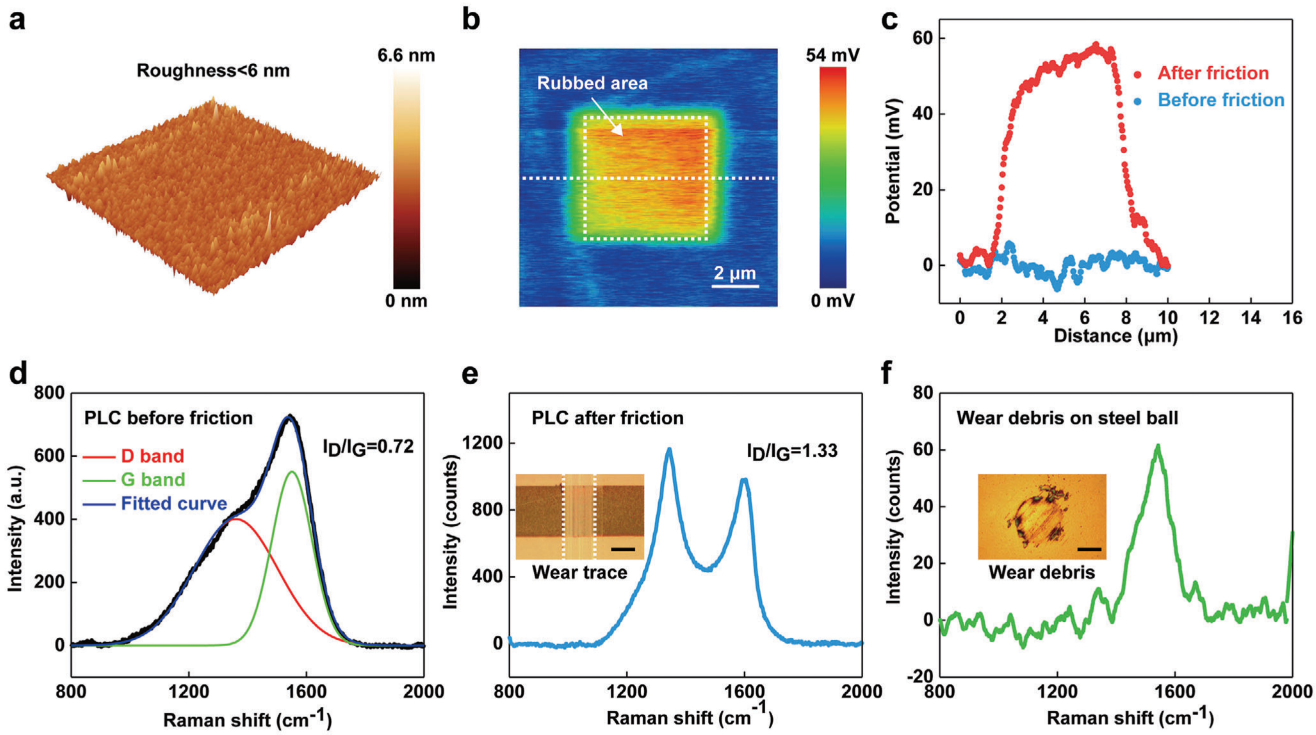

Figure 2. Characterization of the PLC film. a) Surface topography of the as-prepared PLC film. b) Surface potential distribution of the PLC film after triboelectrification. c) PLC surface potential change before and after triboelectrification. Raman spectroscopies of the PLC film d) before and e) after friction. f) Raman spectroscopy of the PLC wear debris on the steel ball.

intrinsic DLC, Si-doped DLC (Si-DLC), and GLC (Graphitic-like DLC) are prepared. By testing the triboelectric properties of the four kinds of DLC films, the PLC is first selected as the superlubric material, which is deposited on the surface to serve as the triboelectric layer of TENG (Figure 1a vii). A spherical external object is used as the sliding friction pair. The detailed fabrication process can be found in Experimental Section. The surface-deposited PLC film is cut by a focused ion beam (FIB) so that the cross-sectional view can be observed, which demonstrates there is no significant height difference between the Cu electrode and SiO_2 substrate (Figure 1b). The flat surface can avoid increased coefficient of friction and wear. The wear trace on the PLC surface and the wear debris on the spherical friction pair were observed by optical microscope after SS-TENG works, which indicates the practical contact area of SS-TENG has a diameter of 130 μm (Figure 1c,d).

The Raman spectrum of DLC films is shown in Figure S1 (Supporting Information), in which it contains various positions of G-Peak and the value of I_D/I_G (ratio of D-Peak intensity to G-Peak intensity) for bringing out the significant difference between the structure and performance. The surface topography of four different kinds of DLC films are characterized by AFM in tapping mode, which indicates the PLC film has a minimum roughness of less than 6 nm (**Figure 2**a; Figure S2, Supporting Information). By coupling the contact-mode AFM and scanning Kelvin probe microscope (SKPM), the triboelectric property of DLC films can be characterized (Figure S3, Supporting Information). At first, an area of 5 × 5 μm on the DLC surface is selected and scanned by AFM tip with platinum (Pt) coating in contact mode to induce nanoscale triboelectrification. Because the Fermi level of the AFM tip is higher than the highest filled surface energy state of DLC, electrons will transfer from the AFM tip to DLC film. Then the surface potential distribution of a larger area of 10 × 10 μm on the DLC surface is measured by SKPM. The measured potential difference between the contact-scanned area and the surrounding area represents the amount of transferred charges during nanoscale triboelectrification (Figure 2b). According to the cross-sectional view of surface potential distribution on DLC films, the PLC film has the maximum potential difference of 55 mV after nanoscale triboelectrification, which means the PLC has the highest ability to obtain electron among the four kinds of DLC (Figure 2c; Figure S4, Supporting Information). In addition, the electric conductivity of PLC film has been measured in Figure S5 (Supporting Information). The *I–V* curve indicates the PLC film is an insulator in this work. Based on the above experimental results, the PLC film was selected as the triboelectric layer of TENG.

During the friction process, due to the different hardness of the two materials, the material with higher hardness will take away the material with lower hardness so that a transfer layer is formed at the friction interface. To understand the superlubric features of the friction interface, the Raman spectrum was characterized. The interesting finding is that Raman spectrum fitting results of the wear track showed an obvious blue shift of G peak and increasing in the ratio of I_D/I_G compared to the PLC film (Figure 2d,e). However, there is only one G peak (1544 cm^{-1}) occurred in the wear debris (Figure 2f), indicating that the friction process causes the construction of a transfer

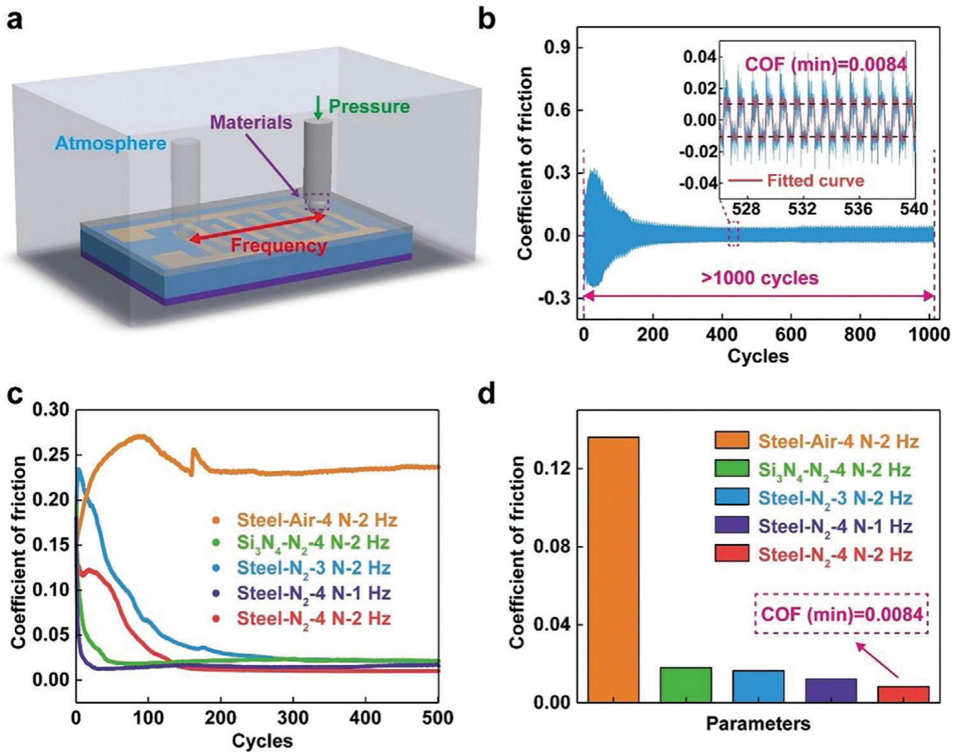

Figure 3. Frictional properties of the SS-TENG. a) Schematic diagram of the friction testing equipment. b) Frictional stability and durability testing at superlubric conditions. c) Variation of friction coefficient with testing time at different parameters. d) Dependence of the minimum friction coefficients on different parameters.

layer in the interface, which is considered the main factor of superlubricity.

To realize the superlubric condition, the frictional property is investigated with different parameters including the material of the spherical friction pair, atmosphere, contact force, and reciprocating motion frequency, which are considered to affect the coefficient of friction (**Figure** 3a). The measurement setup is exhibited in Figure S6 (Supporting Information), in which a spherical friction pair can be controlled to slide back and forth on the surface of the PLC film, and the coefficient of friction can be synchronously measured at different parameters. The measured coefficient of friction depended on sliding cycles at the friction pair material of steel, the atmosphere of N_2, the contact force of 4 N, and the reciprocating frequency of 2 Hz is shown in Figure 3b.

To find out the suitable parameters for superlubric condition, the coefficient of friction is, respectively, measured at five groups of parameters including steel-air-4 N-2, steel-N_2-3 N-2, steel-N_2-4 N-1, Si_3N_4-N_2-4 N-2, and steel-N_2-4 N-2 Hz. The experimental results indicate the coefficient of friction decreases and tends to reach a stable value with the increasing of friction cycles except in air conditions (Figure 3c; Figure S7, Supporting Information). The finally achieved minimum coefficient of friction at different parameters are shown in Figure 3d. When the material of spherical friction pair, atmosphere, contact force, and motion frequency are steel, N_2, 4 N, and 2 Hz, respectively, the minimum coefficient of friction of 0.0084 has been realized, which can be regarded as the superlubirc condition. The stability and durability tests are also shown in Figure 3b, in which the ultralow coefficient of friction of 0.0084 can be maintained over 1000 cycles.

The nanostructures in superlubric interface were characterized by FIB technology (Figure S8, Supporting Information). The transmission electron microscope (TEM) results show the in situ formation of graphene-like a-C:H shear band along the sliding interface, in which atoms undergo friction-induced directed rearrangements (**Figure** 4a,b). The high magnification images of the shear band further reveal the ordering graphene-like structure, in which the layer spacing is ≈0.35 nm (Figure 4c). The friction-induced almost uniform nanostructure of the shear band is the major factor in friction coefficient reduction to achieve a superlubric interface.

Based on the superlubric condition, the electric output was measured. The working principle of SS-TENG is schematically illustrated in **Figure** 5a, in which the interdigital electrodes are simplified to two electrodes on the left and right to analyze the mechanism of power generation. When the bearing-steel ball slides on the PLC surface at superlubric conditions, electrons transfer from the stainless steel ball to the PLC surface, because PLC is easier to obtain electrons compared with AFM tip. When the bearing-steel ball moves to the left electrode, a potential difference is formed across the two electrodes so that the current is generated from the left electrode to the right electrode to realize the state of electrostatic balance. Similarly, the current from right electrode to the left electrode is derived when the bearing-steel ball moves to the right electrode. Thus, the continuous

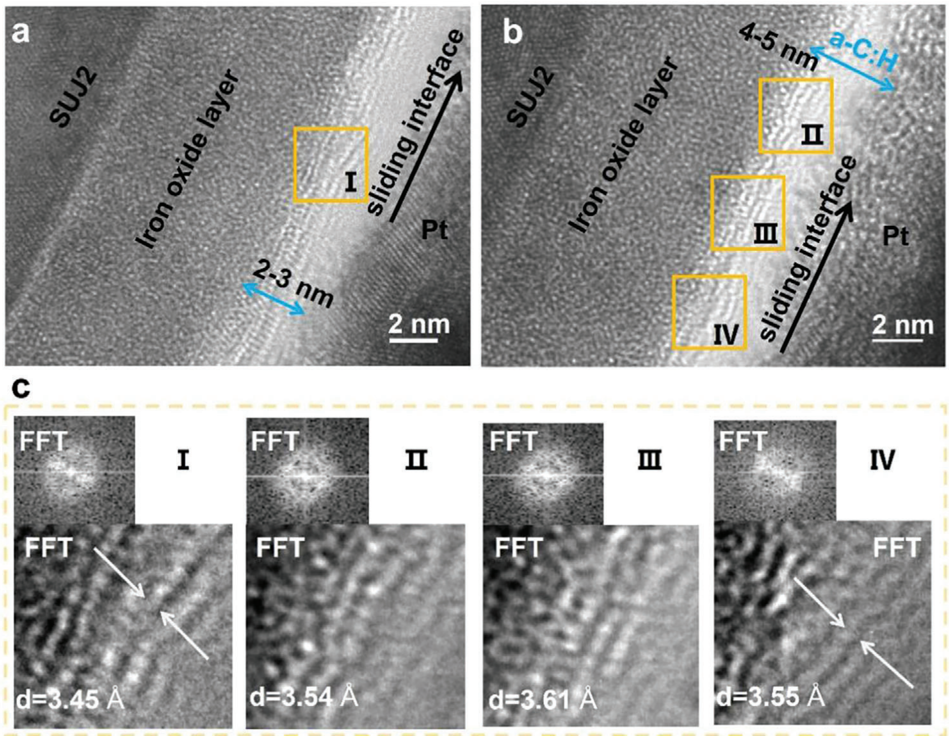

Figure 4. Superlubric interfacial nanostructure. a,b) The in situ formation of the graphene-like shear band on the bearing steel ball surface along the sliding interface. c) High-magnification images showing the ordering graphene-like structures.

alternating current (AC) output can be generated when the bearing-steel ball slides back and forth on the PLC surface.

The electric output at superlubric condition is shown in Figure 5b–d and Table S1 (Supporting Information), in which the SS-TENG has an open-circuit voltage of 40 mV, a short-circuit current of 0.7 nA, and a peak power density of 3 mW m^{-2} with a matching impedance of 4 MΩ. The electric output at the other four groups of parameters, which are not superlubric conditions, is shown in Figure S9 (Supporting Information). There is no significant output decrease between non-superlubric and superlubric states (Figure S10, Supporting Information), which means superlubrication barely affects the power generation. This is very different from the previously reported superlubric generator based on the tribovoltaic effect (Table S2, Supporting Information), in which the superlubric interface leads to a reduction in the injected mechanical energy resulting in a significant decrease of electric output.[30] In addition, according to the stability and durability test, there is no significant decay in the electric output of SS-TENG after 1000 cycles (Figure 5e).

3. Discussion

From the tribological behaviors under the normal loads of 3 to 4 N with various tribopairs, it was confirmed that the hydrogen content and the sp^2 nanoclustering structure of the a-C:H film became a decisive factor for fulfilling the robust superlubricity of SS-TENG in dry nitrogen gas environment. The underlying mechanism regarding the frictional interface of a-C:H film responding to the variable electrostatic balance condition requires a deep investigation. From the results of Raman spectra and TEM observation of the wear scar and its wear debris after the tribotest, it can be found that the microstructure of the sliding interface is closely related to the dynamic changing electrostatic field. The results emphasize that friction-induced formation of sp^2-ordering shear bands with ≈10 nm thickness along the sliding interface is conducive to assisting friction reduction. Furthermore, the dynamic electrostatic field changing triggers the continuous activation of the hydrogenated surface passivation mechanism, which was enhanced by the electrostatic attraction on the interfacial contact area and the increased contact pressure, producing a core contribution to the stability of superlubricity adapted to alternating electrostatic state. Therefore, the as-formed graphene-like shear layers, with the microstructure more like a bonding state of highly-hydrogenated graphitic-like carbon (GLCHH), could provide an easy-shearing lubrication performance with suppressed interfacial material wear loss under the above synergetic effect.[31]

In conclusion, we have developed a superlubric freestanding-mode triboelectric nanogenerator. With the embedded interdigital electrodes and high-quality PLC film as triboelectric layer, the superlubric condition with a coefficient of friction of 0.0084 can be realized, when the material of spherical friction pair, atmosphere, contact force, and reciprocating frequency are steel, N_2, 4 N, and 2 Hz, respectively. At the submillimeter-scale practical contact area of 120 μm, the device can generate an open-circuit voltage of 40 mV, a short-circuit current of 0.7 nA and a maximum power density of 3 mW m^{-2} with a matching impedance of 4 MΩ. Moreover, the device has been demonstrated to be stable and durable, which has no significant change for both the

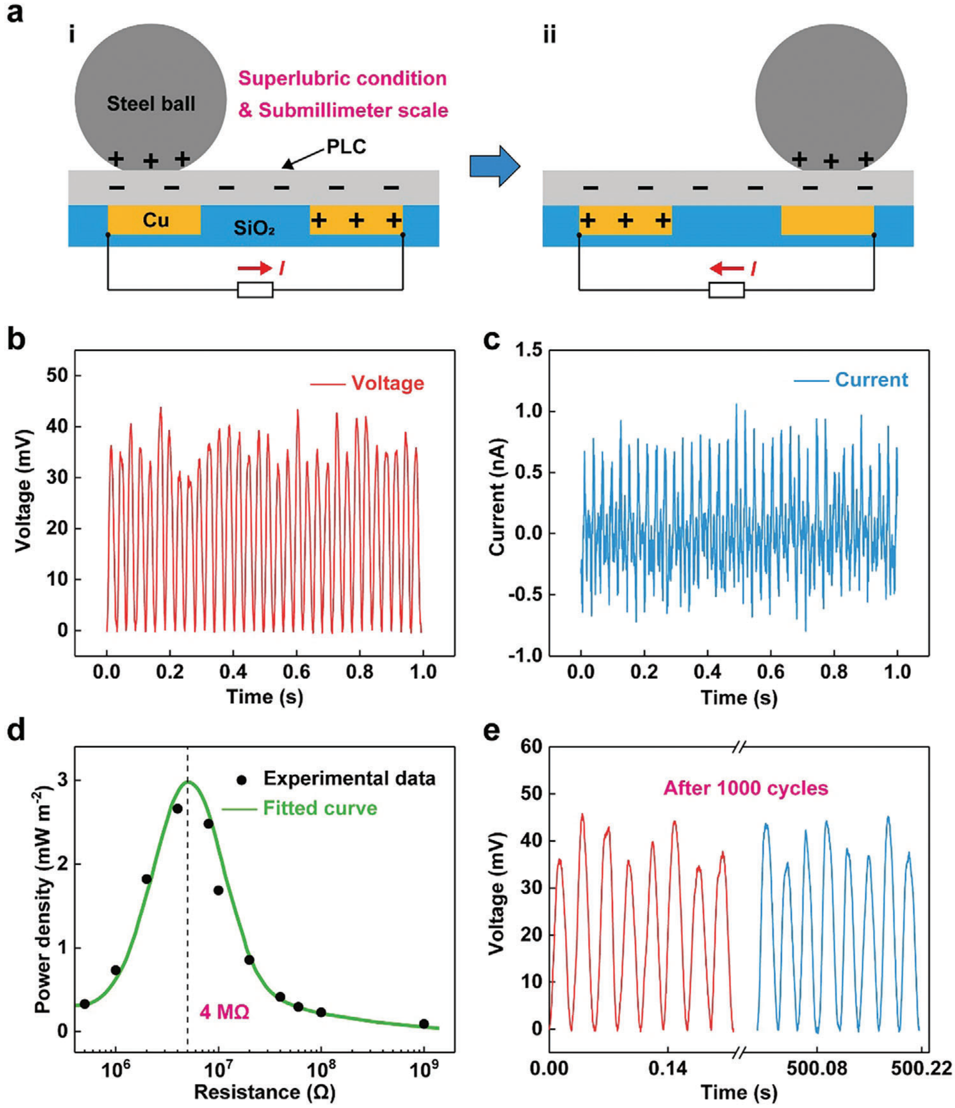

Figure 5. Electric output of the SS-TENG. a) Working mechanism of the SS-TENG. b) Open-circuit voltage and c) short-circuit current of the SS-TENG. d) Dependence of the peak power on different resistive loads. e) Stability and durability testing of the SS-TENG.

coefficient of friction and electric output after 1000 cycles. This work has provided a viable strategy for the development of long-lifetime TENG, which may have great applications in frictional energy recovery from mechanical components, human joint motion, and natural environment.

4. Experimental Section

Fabrication of the SS-TENG: First, a SiO_2/Si wafer was prepared, which has a top 500 nm thick SiO_2 layer. Then, part of the wafer was masked by lithography (SUSS MA/BA 6), and the areas of interdigital electrodes were etched with a depth of 150 nm by inductively coupled plasma (ICP, STS Multiplex AOE). Cu with a thickness of 150 nm was next deposited by RF sputtering (Denton Discovery635). Through the process of lift-off, interdigital electrodes were formed. At last, the top PLC film with a thickness of 900 nm was deposited by an ion-beam deposition system.

Characterization of the SS-TENG: The Raman spectrum was measured by Andor 500i spectroscopy with a 532 nm laser and with a power of 1 mW. The topography of PLC films was characterized by AFM (Asylum Research, MFP-3D) in tapping mode. The triboelectric properties of PLC films were characterized by using contact-mode AFM with a contact force of 10 nN and SKPM for measuring surface potential distribution. The coefficient of friction at different parameters were measured by using a ball-on-disc tribometer (VTRB, Anton Paar), in which the material of the spherical friction pair, atmosphere, contact force, and reciprocating frequency could be controlled, respectively. In detail, the COF of SS-TENG was measured by linear reciprocating motion in the chamber of the tribometer, which was in air condition first. Then the chamber was evacuated by the vacuum pump and nitrogen was passed through to form a nitrogen atmosphere. The COF of SS-TENG was monitored in real-time to investigate the influence of the nitrogen atmosphere. The lamellar specimens prepared for TEM observation were obtained by the FIB system (a focused-ion beam system, LYRA3, Tescan) to figure out the microstructural characteristics of the specified superlubricity micro-zone, which extracted micro-area information about a thickness-less than 100 nm. After that, the as-prepared lamellar atomic-scale structures were carried out by the high-resolution transmission electron microscope system, operating at 200 kV (HRTEM, JEOL 2010F). The electric output of SS-TENG was measured by an electrometer (Keysight 6514).

Supporting Information

Supporting Information is available from the Wiley Online Library or from the author.

Acknowledgements

T.B., W.D., and Y.L. contributed equally to this work. The authors thank the support of the National Key Research and Development (R&D) Program from Ministry of Science and Technology (2023YFB3208100), the National Natural Science Foundation of China (U23A20640, 52105569, 52250112, 52222506), and the Beijing Natural Science Foundation (3222010, 3234057).

Conflict of Interest

The authors declare no conflict of interest.

Data Availability Statement

The data that support the findings of this study are available from the corresponding author upon reasonable request.

Keywords

diamond-like carbon, submillimeter scale, superlubricity, triboelectric nanogenerator

Received: March 6, 2024
Revised: May 13, 2024
Published online: June 5, 2024

[1] H. Chen, M. Ling, L. Hencz, H. Y. Ling, G. Li, Z. Lin, G. Liu, S. Zhang, *Chem. Rev.* **2018**, *118*, 8936.
[2] X. Chen, S. Xu, N. Yao, Y. Shi, *Nano Lett.* **2010**, *10*, 2133.
[3] C. Dagdeviren, P. Joe, O. L. Tuzman, K. Il Park, K. J. Lee, Y. Shi, Y. Huang, J. A. Rogers, *Extreme Mech Lett* **2016**, *9*, 269.
[4] N. E. DuToit, B. L. Wardle, S. G. Kim, *Integr. Ferroelectr.* **2005**, *71*, 121.
[5] A. Erturk, D. J. Inman, *J Intell Mater Syst Struct* **2008**, *19*, 1311.
[6] C. R. Bowen, H. A. Kim, P. M. Weaver, S. Dunn, *Environ Sci* **2008**, *7*, 25.
[7] P. D. Mitcheson, E. M. Yeatman, G. K. Rao, A. S. Holmes, T. C. Green, *Proc IEEE Inst Electr Electron Eng* **2008**, *96*, 1457.
[8] S. R. Anton, H. A. Sodano, *Smart Mater. Struct.* **2007**, *16*, R1.
[9] S. P. Beeby, M. J. Tudor, N. M. White, *Meas. Sci. Technol.* **2006**, *17*, R175.
[10] G. Chen, Y. Li, M. Bick, J. Chen, *Chem. Rev.* **2020**, *120*, 3668.
[11] Z. L. Wang, *ACS Nano* **2013**, *7*, 9533.
[12] Z. L. Wang, J. Chen, L. Lin, *Energy Environ. Sci.* **2015**, *8*, 2250.
[13] C. Wu, A. C. Wang, W. Ding, H. Guo, Z. L. Wang, *Adv. Energy Mater.* **2019**, *9*, 1802906.
[14] J. Chen, Y. Huang, N. Zhang, H. Zou, R. Liu, C. Tao, X. Fan, Z. L. Wang, *Nat. Energy* **2016**, *1*, 16138.
[15] F. R. Fan, Z. Q. Tian, Z. L. Wang, *Nano Energy* **2012**, *1*, 328.
[16] F. R. Fan, W. Tang, Z. L. Wang, *Adv. Mater.* **2016**, *28*, 4283.
[17] H. Wu, Y. A. Huang, F. Xu, Y. Duan, Z. Yin, *Adv. Mater.* **2016**, *28*, 9881.
[18] J. Chen, Z. L. Wang, *Joule* **2017**, *1*, 480.
[19] K. Dong, X. Peng, Z. L. Wang, *Adv. Mater.* **2020**, *32*, 1902549.
[20] Z. L. Wang, T. Jiang, L. Xu, *Nano Energy* **2017**, *39*, 9.
[21] A. Sutka, K. Malnieks, M. Zubkins, A. Pludons, A. Sarakovskis, O. Verners, R. Eglitis, P. C. Sherrell, *ACS Appl. Mater. Interfaces* **2023**, *15*, 33140.
[22] X. Li, X. Yin, Z. Zhao, L. Zhou, D. Liu, C. Zhang, C. Zhang, W. Zhang, S. Li, J. Wang, Z. L. Wang, *Adv. Energy Mater.* **2020**, *10*, 1903024.
[23] H. S. Kim, D. Y. Kim, J. E. Kim, J. H. Kim, D. S. Kong, G. Murillo, G. H. Lee, J. Y. Park, J. H. Jung, *Adv. Funct. Mater.* **2019**, *29*, 1905816.
[24] L. Zhou, Y. Gao, D. Liu, L. Liu, Z. Zhao, S. Li, W. Yuan, S. Cui, Z. L. Wang, J. Wang, *Adv. Energy Mater.* **2021**, 2101958.
[25] S. Li, S. Wang, Y. Zi, Z. Wen, L. Lin, G. Zhang, Z. L. Wang, *ACS Nano* **2015**, *9*, 7479.
[26] W. Xu, X. Zhou, C. Hao, H. Zheng, Y. Liu, X. Yan, Z. Yang, M. Leung, X. C. Zeng, R. X. Xu, Z. Wang, *Natl Sci Rev* **2019**, *6*, 540.
[27] X. Huang, X. Xiang, J. Nie, D. Peng, F. Yang, Z. Wu, H. Jiang, Z. Xu, Q. Zheng, *Nat. Commun.* **2021**, *12*, 2268.
[28] L. Zhang, H. Cai, L. Xu, L. Ji, D. Wang, Y. Zheng, Y. Feng, X. Sui, Y. Guo, W. Guo, F. Zhou, W. Liu, Z. L. Wang, *Matter* **2022**, *5*, 1532.
[29] N. Ohtake, M. Hiratsuka, K. Kanda, H. Akasaka, M. Tsujioka, K. Hirakuri, A. Hirata, T. Ohana, H. Inaba, M. Kano, H. Saitoh, *Materials* **2021**, *14*, 315.
[30] Z. Wang, K. Gao, Y. Feng, J. Cao, L. Gong, B. Fan, Y. Zhang, G. Xie, C. Zhang, *Sci. Bull.* **2024**, *69*, 1197.
[31] C. Casiraghi, A. C. Ferrari, J. Robertson, *Phys. Rev. B* **2005**, *72*, 085401.